BNL-NUREG-35285
CONF-8406124--14

NONLINEAR FAILURE ANALYSIS OF A REINFORCED CONCRETE CONTAINMENT UNDER INTERNAL PRESSURE

S. Sharma, Y.K. Wang and M. Reich
Structural Analysis Division
Upton, NY 11973

BNL-NUREG--35285

TI85 000877

ABSTRACT

A detailed nonlinear finite element model is used to investigate the failure response of the Indian Point containment building under severe accident pressures. Refined material models are used to describe the complex stress-strain behavior of the liner and rebar steels, the plain concrete and the reinforced concrete. Structural geometry of the containment is idealized by eight layers of axisymmetric finite elements through the wall thickness in order to closely model the actual placement of the rebars. Soil stiffness under the containment base mat is modeled by a series of nonlinear spring elements. Numerical results presented in the paper describe cracking and plastic deformation (in compression) of the concrete, yielding of the liner and rebar steels and eventual loss of the load carrying capacity of the containment. The results are compared with available data from the previous studies for this containment.

1. INTRODUCTION

Structural integrity of nuclear containments under severe accidental pressures due to hydrogen burn following a postulated loss of coolant accident has received considerable attention in recent years. For reinforced concrete containments several detailed analysis results have appeared in the literature. A comparison of the results, however, shows that different failure mechanisms and failure pressures have often been predicted for the same containment. Essentially, the structural failure is either due to shear failure of the concrete at the cylinder-basemat junction, or from the failure of the hoop reinforcement, located below the dome-cylinder junction. The predicted pressure for shear failure is considerably lower than the pressure calculated for hoop reinforcement failure.

The different answers can be attributed due to differences in structural models, especially, in the non-linear models used for the concrete. In order to correctly predict shear failure in concrete, it is necessary to employ a reliable material model that can represent siginficant plasticity in compression, fracture in both compression and tension, and the complex interactions that occur between the cracked concrete and the rebars. In this paper the failure mechanism of a typical reinforced concrete containment i.e., the containment for the Indian Point Unit 3 Reactor, is evaluated using a detailed finite element model in which the material modeling aspect is emphasized. Comparisons with results in the literature are made.

2. CONTAINMENT STRUCTURE

The Indian Point, Unit 3, containment building (Fig. 1) is a conventionally reinforced concrete structure consisting of three basic parts: (1) a base mat, (2) a circular cylinder, and (3) a hemispherical dome. The base mat is a 9 ft. thick circular slab with a sump at the center. The outer

DISCLAIMER

diameter of the slab is 145.8 ft. The 4.5 ft. thick cylindrical wall has an internal diameter of 135 ft. and a height of 148 ft. as measured from the top of the base mat to the dome-cylinder junction (springline). Above this junction the containment is capped by the hemispherical dome which has the same internal diameter (135 ft.) as the cylinder, but a reduced wall which is equal to 3.5 ft.

The interior surface of the containment is lined with a ductile steel (ASTM A442 Grade 60) liner of varying thickness. Its thickness is 0.25 in. in the dome section and at the bottom 30 ft. section of the cylinder. The thickness the remaining sections of the cylinder is 0.38 in.

Reinforcing bars (nominal yield stress of 60 ksi) of various sizes, mainly #18, #14 and #11, are placed in different patterns and spacings to reinforce the containment building. The primary membrane reinforcement in the cylindrical wall and dome is divided into two equal groups placed near the inside and outside faces of the containment wall. Each group consists of two layers of hoop bars and one layer of meridional bars as depicted in Fig. 2. In addition, a layer of helical bars at +45° and -45° with the vertical axis is placed near the outside face to resist in-plane shear forces. These bars extend from the top of the base mat to the bottom third of the dome. Further details pertaining to the reinforcing bar sizes and spacings can be found in Ref. [1].

3. MATERIAL MODELS

As mentioned previously, in order to predict the containment failure mechanism and failure response, nonlinear materials models that can accurately describe the complex stress-strain behavior of the concrete and steels must be used. The material models used in the present finite element analysis are discussed in this section.

3.1 Steels

A von Mises plasticity model with an isotropic strain hardening rule was adopted to represent the nonlinear response of the liner and reinforcement steels. Since this is a well-known material model, only the major equations are briefly outlined.

Under the influence of current stresses σ_i, i = 1, 2, ... 6, the state of deformation a steel element is defined by a loading function f_s of the form

$$f_s = \frac{1}{2} S_i^T S_i - \kappa^2 = 0 \qquad (1)$$

where S_i and S_i^T denote the stress deviator and its transpose, respectively, and κ is a function of plastic work, W_p:

$$\kappa = \kappa (W_p) \qquad (2)$$

and

$$W_p = \int \sigma_i \, d\varepsilon_i^p \qquad (3)$$

where ε_i^p are the plastic strain components.

The incremental plastic strain components are given by the following flow rule

$$d\varepsilon_i^p = d\lambda \quad \frac{\partial f}{\partial \sigma_i} \tag{4}$$

where $d\lambda$ is a plastic parameter. Following the standard procedure used in plasticity theory, an incremental stress-strain relation in matrix form can be derived from Eqs. (1) to (4) as

$$\{d\sigma\} = \left[C_{EP}^1\right] \{d\varepsilon\} \tag{5}$$

where $\left[C_{EP}^1\right]$ is an elastic-plastic matrix of the steel element.

3.2 Plain Concrete

The nonlinear material behavior of plain concrete is characterized by two main features: i) some plastic deformation before crushing under high compressive stresses, and ii) cracking under relatively low tensile stresses. These features can be represented by an elastic-plastic model combined with a fracture criterion for crushing and cracking.

Elastic-plastic Model - An elastic-plastic model orignated by Chen and Chen [2] was used for the present analysis. It predicts the nonlinear concrete behavior with sufficient accuracy, and is formulated in a manner that allows for implementation in finite element programs. This model defines two different but similar loading functions to describe the yielding of concrete in different stress regions.

Compression-compression stress state:

$$f_c = \frac{J_2 + (\beta/3)\, I_1}{1 - (\alpha/3)\, I_1} = \tau^2 \tag{6}$$

Tension-compression o tension-tension stress state:

$$f_c = \frac{J_2 - \frac{1}{6}\, I_1^2 + (\beta/3)\, I_1}{1 - (\alpha/3)\, I_1} = \tau^2 \tag{7}$$

where α and β are material constants and τ is a strength parameter [2]. J_2 is the second invariant of stress deviator, and I_1 is the first invariant of stress components. Initial and subsequent loading surfaces defined by Eqs. (6) and (7) are shown in Fig. 3. With these loading functions and the flow rule given by Eq. (4), an incremental stress-strain relationship for the concrete can be derived as

$$\{d\sigma\} = \left[C_{EP}^2\right] \{d\varepsilon\} \tag{8}$$

where $\left[C_{EP}^2\right]$ is an elastic-plastic material matrix for the concrete [2].

Fracture of Concrete - A dual fracture criterion in terms of both stresses and strains is used. The stress-based criterion is obtained simply

$$g(\varepsilon_i) = J_2(\varepsilon) + \frac{A_u}{3}\frac{\varepsilon_u}{f'_c} I_1(\varepsilon) = (\tau_u)^2 \left(\frac{\varepsilon_u}{f'_c}\right)^2 \quad (9)$$

or

$$\varepsilon_{max} = \varepsilon_t \quad (10)$$

where $J_2(\varepsilon)$ is the second invariant of strain deviator; I_1, the first invariant of strain components; f'_c, uniaxial compressive strength of concrete; A_u, a material constant; ε_u, ultimate compressive strain; ε_t, ultimate tensile strain and ε_{max}, maximum principal strain obtained from the analysis. The fracture surface in a biaxial strain plane is shown in Fig. 4.

When the concrete fractures in a compressive stress state (crushing), its stiffness and stresses in all directions are set to zero. In the case of tensile fracture (cracking), however, only those stiffness and stress terms that are associated with the normal to the cracked plane are gradually reduced to specified minimum values. The gradual reduction of these terms as a function of the strain normal to the cracked plane is carried out in the present analysis in order to represent such effects as tension-stiffening and loss of shear strength in the cracked concrete.

3.3 Reinforced Concrete

Reinforcing bars in the concrete can be modeled either discretely as truss or beam elements, or in a distributed sense in which the reinforced concrete is treated as a composite material. The latter approach is computationally more efficient and in addition can model the concrete steel interaction effects more accurately. In the present analysis, a consistent smearing procedure [3,4] has been used to idealize the reinforced concrete as an equivalent nonlinear composite material. Essentially, the smearing procedure assumes that specified components of strains and stresses are uniform in both the concrete and steel. The incremental constitutive matrix for the reinforced concrete can then be derived as a function of stress, strain and constitutive matrices for both of its constituents, concrete and steel. Similarly, once the overall deformation of the smeared reinforced concrete is obtained, a de-smearing procedure (an inverse process to the smearing procedure) can be used to calculate stresses and strains in the concrete and steel. The stresses and strains are then used to assess the yielding of steel or fracture of concrete. A detailed description of the smearing approach for elastic-plastic composites with a derivation of relevant equations is given in Ref. [4].

4. FINITE ELEMENT MODEL

The containment building is assumed to be axisymmetric for the finite element idealization. The effect of containment penetrations, which are non-axisymmetric, is ignored in this analysis since it is mainly aimed at determining the global response of the containment. This simplification with

respect to the penetrations is justified since the penetrations are small when compared to the containment size. Furthermore, areas around the penetrations are provided additional reinforcement to prevent any localized failure. All steel reinforcements, including vertical and diagonal rebars, are assumed to be axisymmetric in a distributed sense. This is also a valid approximation in view of the smearing and de-smearing procedures used for modeling the reinforced concrete.

The finite element model of the containment, shown in Figure 5, was constructed using a nonlinear finite element code, NFAP, developed at the Brookhaven National Laboratory. The model consists of 407 eight-noded axisymmetric elements resulting in a total of 1399 nodes. In addition, a set of nonlinear spring elements (high stiffness in compression and zero stiffness in tension) were used under the base mat in order to model the soil restraint and to allow uplifting of the base mat. As shown in the figure, the model has 8 layers of axisymmetric elements in both the cylindrical wall and the hemispherical dome, and 6 layers in most of the base mat. The element layers are chosen to represent separately the liner, the plain concrete, and the reinforced concrete with different reinforcing bars. The spacings and sizes of the layers are selected to model the actual placement of the reinforcements. For the liner and reinforcing steels, Young's modulus of elasticity and Poisson's ratio were taken to be 29,000 ksi and 0.3, respectively. As-built values for the mean yield strength, 48.4 ksi for the liner and 69.7 - 71.0 ksi for various rebars, were used. A bi-linear stress-strain idealization with a plastic tangent modulus of 100 ksi was used for all steels. Material parameters for the plain concrete as required by the Chen and Chen [2] model are given below:

Young's modulus = 3,700 ksi
Poisson's ratio = 0.19
Yield strength in uniaxial tension = 0.216 ksi
Yield strength in uniaxial compression = 1.8 ksi
Yield strength in biaxial compression = 2.160 ksi
Fracture strength in uniaxial tension = 0.4 ksi
Fracture strength in uniaxial compression = 4.0 ksi
Fracture strain in tension = 0.000125
Fractuare strain in compression = 0.003

5. ANALYSIS RESULTS

The loads considered in the analysis were the dead weight or gravity loads and internal pressure. The entire gravity loads were applied to the containment in the first load step at the beginning of the analysis. The internal pressure was, however, incrementally applied. The pressure increments were 1 psig following the onset of nonlinear response. In the nonlinear range, a Newton-Raphson procedure with stiffness reformation for each equilibrium iteration was used to obtain convergent solutions.

5.1 Deformation Response

Undeformed and deformed (before failure) shapes of the containment are depicted in Fig. 6. For clarity, the displacements for the deformed shape are multiplied by a factor of 50. The figure shows large bending deformations at

the cylinder - base mat junction, and comparatively large radial displacements in the middle of the cylindrical wall. The deformations of the base mat indicate that up-lifting occurs below the cylindrical wall at the junction.

The growth of the deformation field is illustrated in Fig. 7 where radial displacements at mid-cylinder and vertical displacements at the top of the dome are plotted versus internal pressure. As can be seen, the displacements are small until tension cracks develop in the concrete at, internal pressure between 25-33 psig (see below). The displacements then grow more rapidly as the concrete loses its load carrying capacity. The rates at which these displacements increase are then controlled by the stiffnesses of the steel members and by the tension-stiffening effect of the cracked concrete.

5.2 Cracking and Shear Failure of Concrete

Vertical cracks due to hoop stresses first appear in the middle of the cylindrical wall at 25 psig. The cracks spread quickly with increasing pressure covering almost the entire length of the cylinder at 26 psig. Only a small section above the cylinder - mat intersection remain uncracked. The hoop strains are very low in this region due to the radial constraints provided by the base mat. As the pressure increases to 29 psig, perpendicular cracks due to both hoop and meridional stresses are initiated in the entire section of the dome.

The next set of cracks appear at the cylinder - mat intersection when the pressure reaches 33 psig. These cracks are due to high tensile meridional stresses and shear stresses in the elements at the inside of cylinder wall which arise as a result of large bending deformations at the intersection. The cracks are formed at some small angles from the horizontal plane because of the combined effect of tensile and shear stresses. The cracking progresses through the intersection with increasing pressure reaching the middle of the intersection (i.e., the cylindrical wall thickness) at 48 psig. At this pressure, horizontal cracks due to meridional stresses also in the entire cylindrical wall except in the outside of the wall near the intersection. The concrete in the region is under compression because of the bending deformations. As the internal pressure is increased further from 48 to 77 psig, the cracked regions expand slowly but essentially with the same crack configurations. Above 77 psig, high shear stresses at the cylinder - mat intersection introduce another set of cracks perpendicular (approximately) to the original cracks in this region. When this occurs, the concrete is assumed to fail in shear and its shear stiffness is greatly reduced. In the present analysis, ten percent of the uncracked shear stiffness is retained in order to approximately represent the cumulative effect of interface shear transfer, dowel mechanism and the stiffness contributions from the reinforcement ties and stirrups.

Shear failure of the concrete progresses through the wall with increasing pressure. At 110 psig, 50 percent of the intersection has failed in shear. The extensive cracking relieves some of the bending moment and shear force in this region. The depth of shear failure, however, keeps increasing, reaching the outside face meridional bars (72 percent of the wall thickness) at 125 psig. Above this pressure (i.e., at 126 psig), a convergent numerical solution could not be obtained. This indicates that the cylinder - mat intersection cannot carry any further increase in the load.

Plasticity of concrete in compression is initiated at 110 psig in some elements at the cylinder base on the outer surface. The plastic zone spreads to neighboring elements with increasing pressure. However, the effective stress in all these elements remains considerably below the fracture strength of the concrete in compression (4 ksi) even at the peak pressure of 125 psig.

5.3 Liner and Rebar Stresses at Cylinder-Mat Intersection

Meridional stresses in both the liner and inside vertical rebars at the cylinder-mat intersection are depicted in Fig. 8. These stresses grow linearly at a slow rate until the concrete begins to crack at 29 psig. The stresses then grow rapidly with pressure to 84 psig as the cracks progress through the wall and the concrete meridional loads are transferred to the steel members. At 84 psig, 7 psig above the pressure at which a second set of cracks develop at the intersection (77 psig), the liner become fully plastic. Additional meridional stresses above 84 psig presssure are carried mainly by the inside vertical rebars, and to some extent by the small section of intact concrete. As shown in the figure, the rebar stresses grow at an even higher rate after the liner has become plastic. Finally, the rebars become plastic at 120 psig. This is soon followed by the shear failure at the intersection at 126 psig as discussed previously.

5.4 Liner and Rebar Stresses at Cylinder Mid-Height

Hoop stresses in the containment are greatest at the cylinder mid-height, at an elevation of 114 ft. For a section at this elevation, hoop stress versus internal pressure curves for the liner, hoop rebars and diagonal rebars are plotted in Fig. 9. The stresses in all the steel members are low until the onset of cracks due to hoop stresses at 25 psig. Above this pressure and up to 104 psig, the stresses grow almost linearly with increasing pressure. Note that the hoop stress in the liner, because of the multi-axial stress state, is higher than that in the hoop rebars in this pressure range. Also, the hoop stress in the diagonal rebars is much lower (approximately 25 percent) since they are inclined 45° to the horizontal axis.

The liner becomes plastic at 104 psig under combined hoop and meridional stresses. Additional hoop stresses are then transferred to the hoop and diagonal rebars as shown in the figure by the higher growth rates of hoop stress versus pressure. Both the hoop and diagonal rebars, however, remain elastic up to 125 psig internal pressure. Analysis results could not be obtained above this pressure because of the shear failure at the cylinder-mat intersection.

5.5 Comparison with Results in the Literature

Finite element analysis results for the failure of Indian Point containment building have been presented previously by Von Riseseman, et al [5], Fardis, et al [6], and Butler and Fugelso [7]. In the first two studies, the containment failure is predicted to result from the yielding of steel members due to large hoop stresses near the cylinder mid-height. References [5] and [6] do not provide any details for the cracking and post-cracking behavior of the concrete. Also, the results presented do not discuss any shear failure of the concrete at the cylinder-mat junction. This may be due to the reason that very simple materials models are used in [5] and [6] to

represent the nonlinear stress-strain response of the concrete. These models may not, therefore, be able to adequately describe the complex plasticity and cracking behavior at the intersection.

Numerical results in [7] were obtained with a computer code ADINA [8] which has a more realistic concrete model. This nonlinear model allows for cracking in tension, crushing in compression and strain-softening. The overall containment failure response described in [7] is in reasonably good agreement with the results described in this paper. The shear failure at the cylinder-mat intersection is predicted at 118 psig as compared with 126 psig in the present analysis. There are, however, two notable differences in the two analyses: (1) only large plastic deformations of concrete on the outside of the wall near the cylinder base are obtained in this study in contrast with significant compression crushing (and corresponding stress increase in rebars) predicted in [7], and (2) the calculated base mat uplift from the present analysis is 1.8 in. at 118 psig which is considerably less than 4.4 in obtained in [7].

6. CONCLUSIONS

Analysis results based on a detailed nonlinear finite element model have been presented in the paper for the failure behavior of the Indian Point containment building. The results show that the cracking of concrete begins in the cylindrical wall due to hoop stresses, and at the cylinder-mat junction due to meridional and shear stresses at 25 and 33 psig, respectively. Secondary cracks on the inside of the intersection develops at 77 psig initiating a loss of concrete shear strength. The transfer of concrete stresses to the steel members in this region leads to the yielding of the liner at 84 psig, and subsequently that of the inside vertical rebars at 120 psig. Further increase in the internal pressure to 125 psig propagates the shear failure at the intersection up to the outside reinforcement bars (72 percent of the wall thickness). The intersection is then unable to carry any further increase in the loads. At the cylinder mid-height, the liner yields at 104 psig, but both the hoop and diagonal rebars remain elastic even at the peak pressure of 125 psig.

REFERENCES

1. "Indian Point Nuclear Power Plant, Unit 3, Final Safety Analysis Report", Docket 50286.

2. Chen, A.C.T. and Chen, W.F., "Constitutive Relations for Concrete", Journal of the Engineering Mechanics Division, ASCE, 101(1975), pp. 465-481.

3. R. Hill, "Theory of Mechanical Properties of Fibre-Strengthened Materials: I. Elastic Behavior," Journal of Mechanics and Physics of Solids, 12(1964).

4. Chang, T.Y. and Aoki, H., "A Constitutive Model for Structural Analysis of Fusion Magnets", Nuclear Engineering and Design, 58(1980), pp. 237-245.

5. Von Riesemann, W.A., Huerta, M., Chen, E-P. and Swenson, D.V., "Structural Response of the Indian Point 2 and Indian Point 3 Containment Buildings", Section 3.2, Report of the Zion/Indian Point Study: Vol. 1, Prepared by W.B. Murfin, Sandia National Laboratory, Albuquerque, NM, Report No. NUREG/CR-1410, SAND80-0617/1, August 1980.

6. Fardis, M.N., Nacar, A. and Delichatsios, M.A., "Reinforced Concrete Containment Safety Under Hydrogen Explosion Loading", Report No. NUREG/CR-2898, U.S. Nuclear Regulatory Commission, Washington, DC, September 1982.

7. Butler, T.A. and Fugelsc, L.E., "Response of the Zion and Indian Point Containment Buildings to Severe Accident Pressure", Report No. NUREG/CR 2569, U.S. Nuclear Regulatory Commission, Washington, DC, May 1982.

8. Bathe, K.J., "ADINA: A Finite Element Program for Automatic Dynamic Incremental Nonlinear Analysis", Report 82448-1, Acoustics and Vibration Laboratory, Dept. of Mechanical Engineering, Massachusetts Institute of Technology, Cambridge, MA, 1978.

This work was performed under the auspices of the U.S. Nuclear Regulatory Commission, Washington, DC.

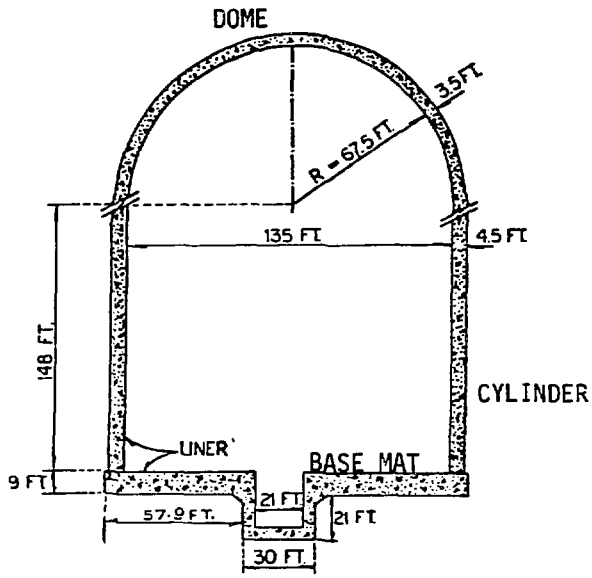

Figure 1 Indian Point Containment Building

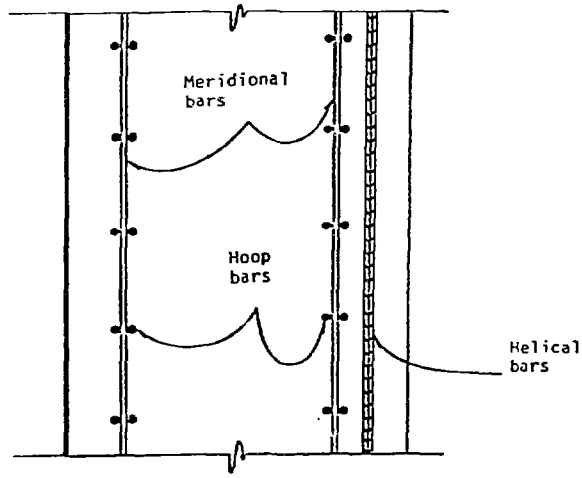

Figure 2 Reinforcement Bars in Cylindrical Wall

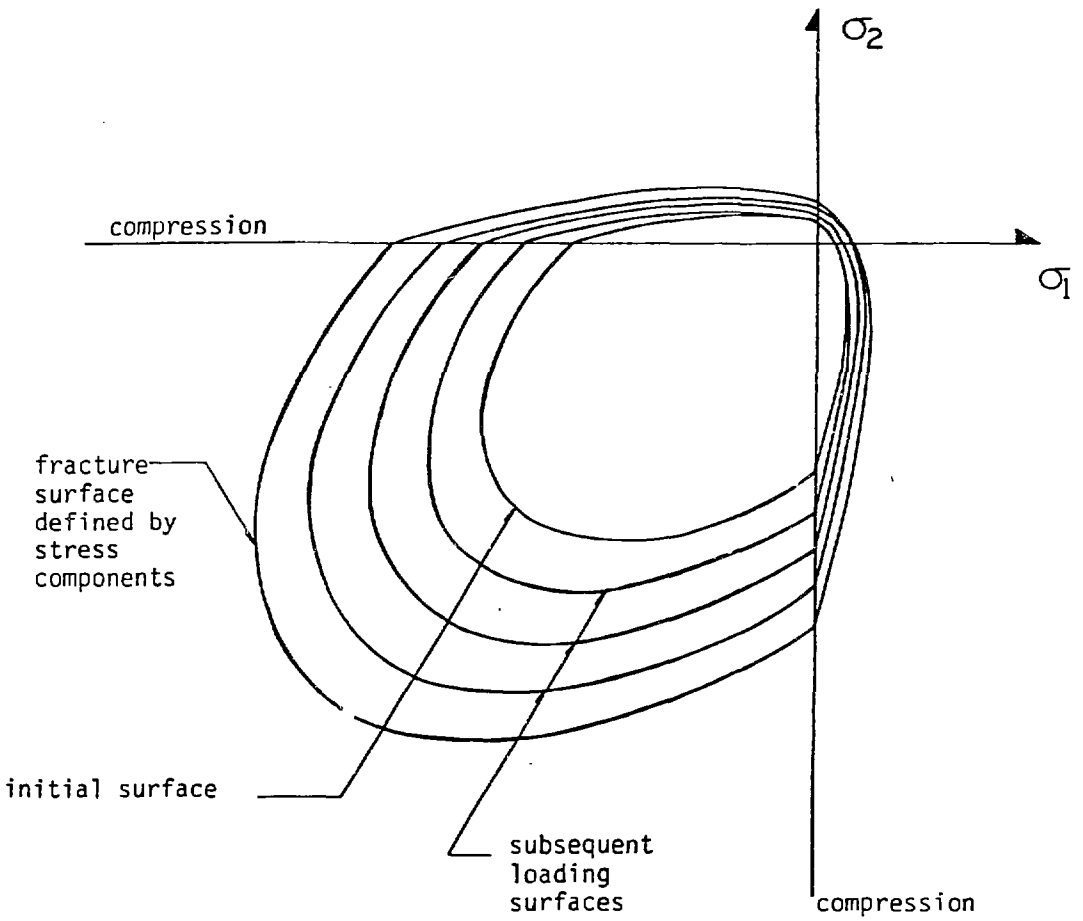

Figure 3 Loading and Fracture Surfaces of Concrete in Biaxial Stress Plane

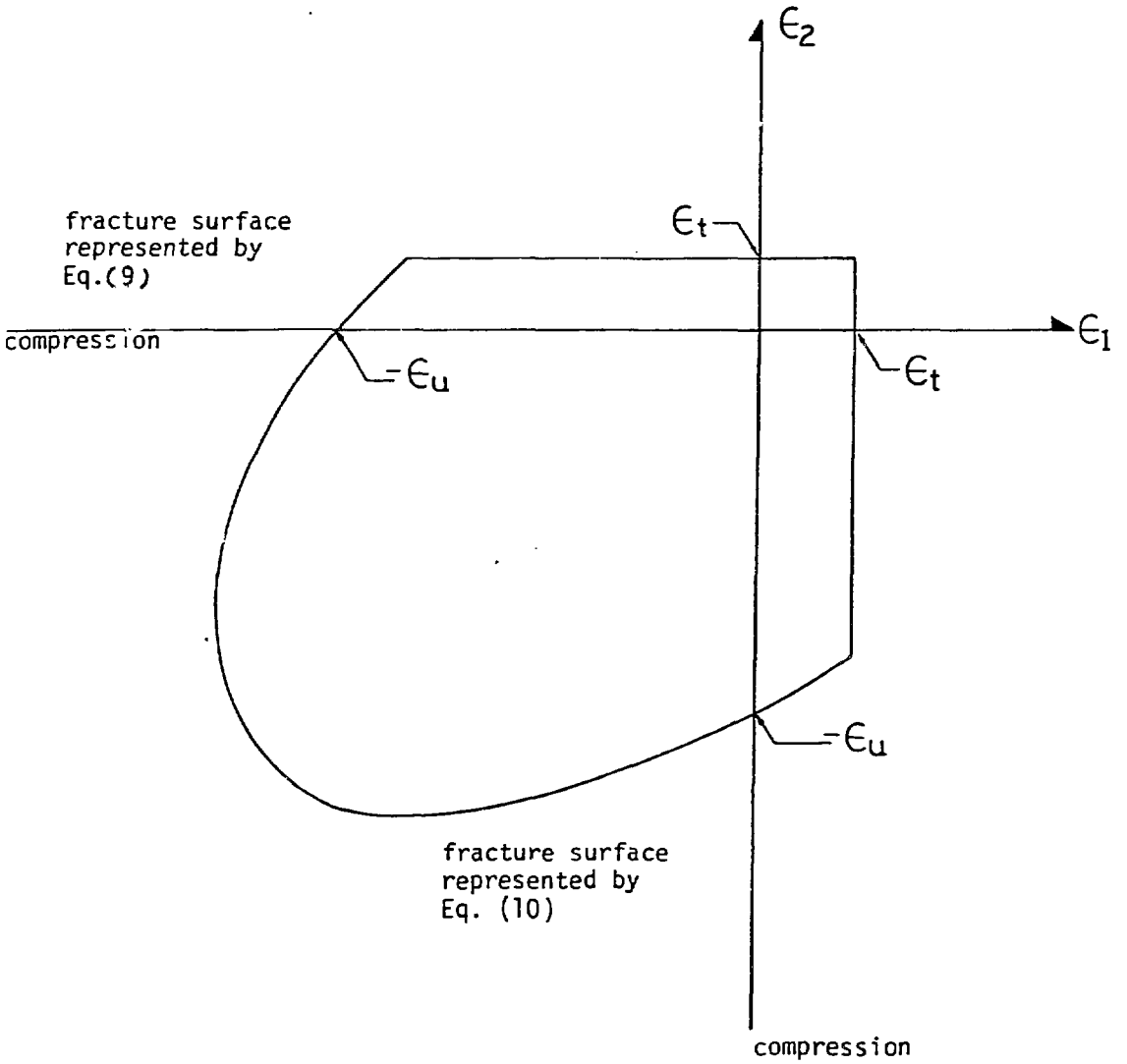

Figure 4 Fracture Surface of Concrete in Biaxial Strain Plane

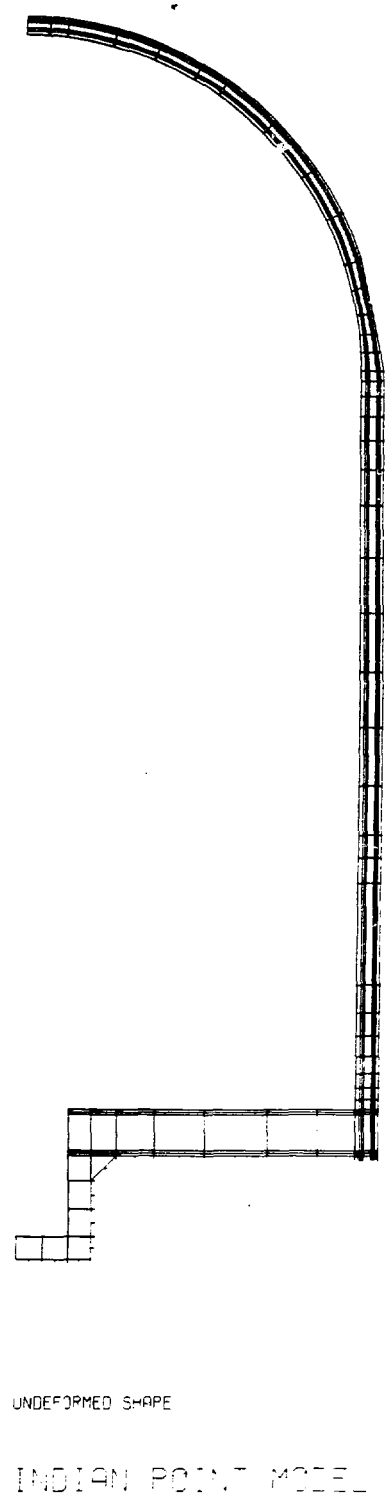

Figure 5 Finite Element Idealization of the Indian Point Containment Building

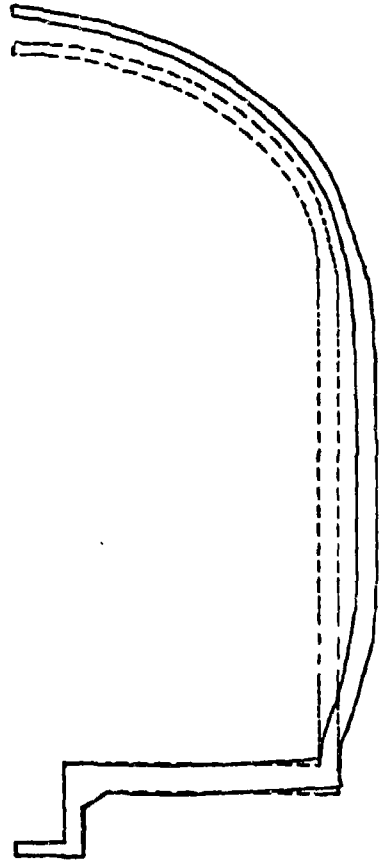

Figure 6 Undeformed and Deformed Shapes of the Indian Point Containment Building

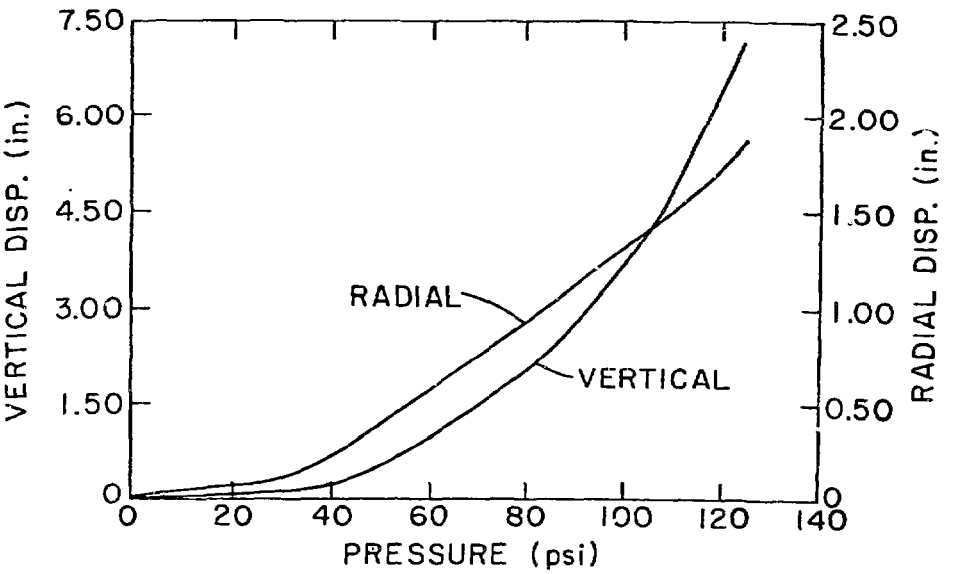

Figure 7 Radial Displacement at Cylinder Mid-Height and Vertical Displacement at Dome Apex Versus Pressure

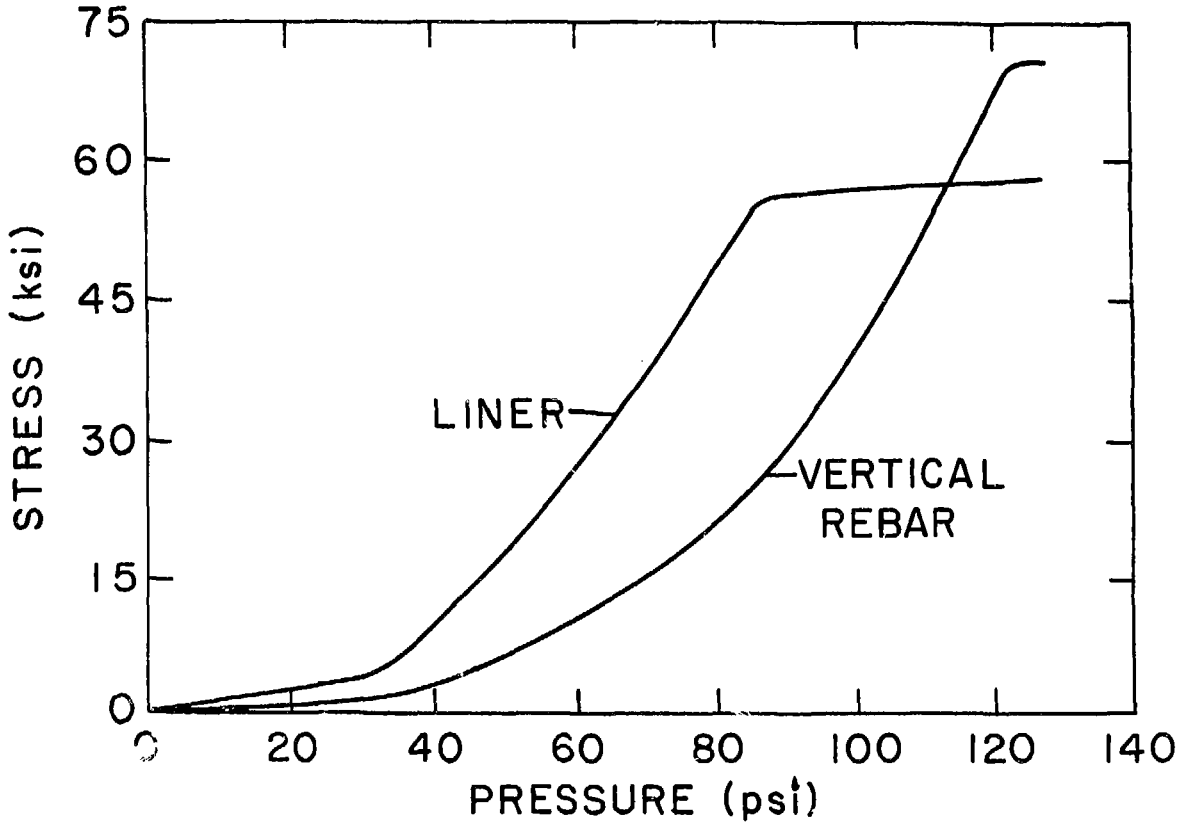

Figure 8 Meridional Stresses in the Liner and Inside Vertical Rebars Versus Pressure

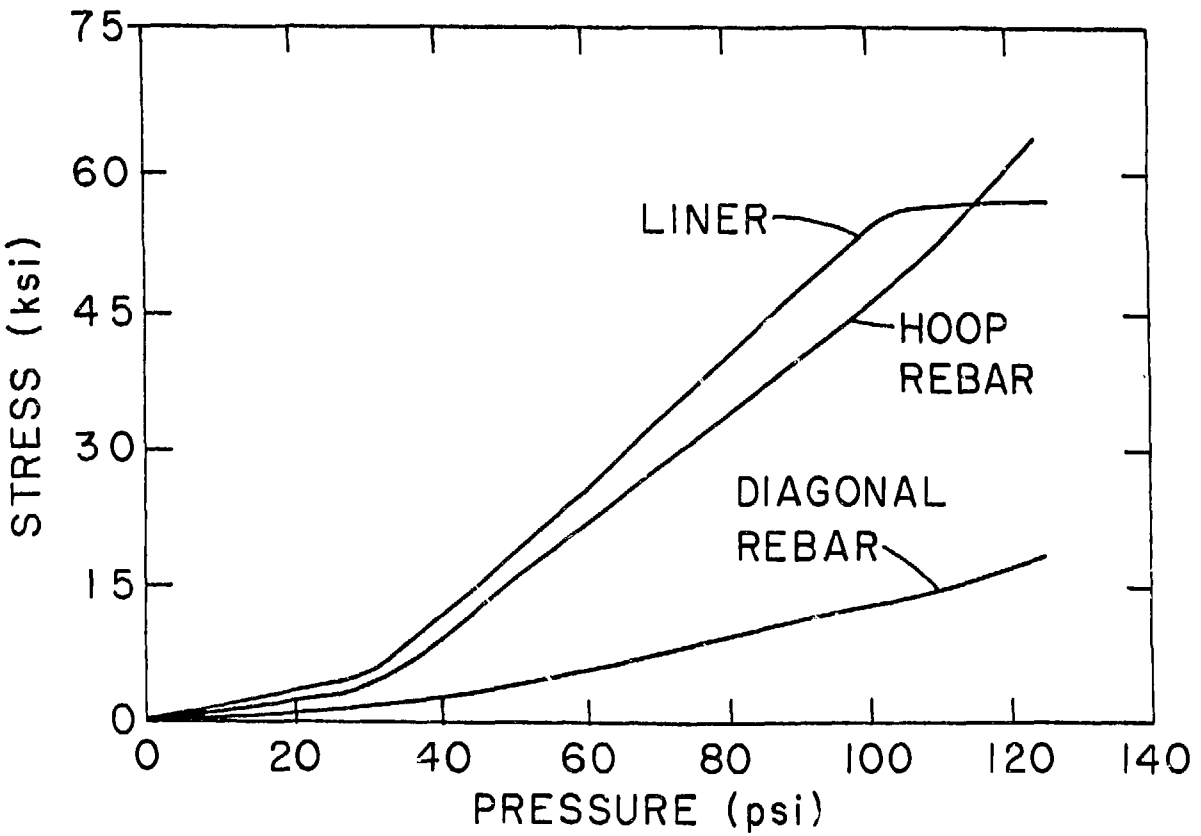

Figure 9 Hoop Stresses in the Liner, Hoop Rebars and Diagonal Rebars Versus Pressure